Experimental Tests and Numerical Modeling of Submerged Wave Attenuators Made of Cages Filled with Oyster Shells in Shallow Water

Michel Benoit, Bernard Molin, Fabien Remy, Nathalie Durand

Conference Paper, Published Version

Benoit, Michel; Molin, Bernard; Remy, Fabien; Durand, Nathalie

Experimental Tests and Numerical Modeling of Submerged Wave Attenuators Made of Cages Filled with Oyster Shells in Shallow Water

Coastal Structures 2019 - Nils Goseberg, Torsten Schlurmann (eds) - © 2019 Bundesanstalt für Wasserbau
ISBN 978-3-939230-64-9 (Online) - DOI: 10.18451/978-3-939230-64-9_016

Experimental Tests and Numerical Modeling of Submerged Wave Attenuators Made of Cages Filled with Oyster Shells in Shallow Water

M. Benoit, B. Molin & F. Remy
Aix Marseille Univ., Centrale Marseille, CNRS, Irphé (UMR 7342), Marseille, France

N. Durand
EDF R&D, Chatou, France

Abstract: In order to reduce wave agitation in shallow-water coastal or lagoon areas, dissipative submerged porous structures made of parallelepipedic metallic cages filled with used oyster shells (COS) are considered. The present study combines an experimental study in an hexapod facility to determine the parameters which best characterize these COS units considered as an homogeneous porous medium. Various numerical modeling strategies are then considered to simulate the propagation of monochromatic waves over a series of such COS devices in water of variable depth. Finally, the results from these models are compared with an independent series of experiments performed in a wave flume with the same COS. Overall, a fair agreement is obtained from these models regarding wave height attenuation and transmission for a range of relative water depth conditions and various relative heights of the COS structures relative to the water depth.

Keywords: water waves, wave attenuation, porous medium, numerical modeling, cage of oyster shells

1 Introduction and scope of the study

In order to promote the growth or spatial extension of certain types of marine vegetation in coastal zones or lagoon areas it is often desired to reduce the local wave-induced agitation due to incident swell and/or wind-seas. In principle, various coastal engineering solutions could be considered for this purpose, including submerged breakwaters, patches of artificial vegetation-inspired flexible or rigid structures, etc. In the present project, we consider an environmental friendly solution using parallelepipedic metallic Cages filled with (used) Oyster Shells (abbreviated COS hereafter), developed by the Ecocean company (France). These modules can be used individually or as combinations of several units. In the application considered here, the COS are laid on the sea bottom in shallow water. These COS constitute an anisotropic porous medium, in which wave energy is dissipated.

With the aim to improve our knowledge of the dissipative mechanisms inside the COS and to develop numerical modeling tools that could be used to help designing coastal protection solutions based on these COS units, the present study combines a series of experimental tests and the development and test of simplified numerical models.

The paper is organized as follows: in Section 2, the general strategy for modeling the wave induced flow in a system composed of a lower layer of homogeneous porous medium (here the COS) and an upper layer of pure water is recalled. In particular, the linear solution for progressive waves in a medium with constant water depth and porous layer height is discussed, together with the associated dispersion relation. In Section 3, we present the experimental campaign carried out with these COS units in an hexapod facility to estimate the values of the parameters which characterize the COS. In Section 4, various modelling strategies for waves interacting with a series of COS are introduced. In particular, two models are selected: one based on the Elliptic Mild Slope (EMS) equation following Rojanakamthorn et al. (1990) and Loasada et al. (1996), and one simplified phase-averaged model, assuming progressive waves. These models are compared to a dedicated series of experiments performed in a wave flume in Section 5. Conclusions are summarized in Section 6.

2 Brief review of flow modeling approach inside and above a porous layer on the bottom

2.1 General modeling of the flow in the porous medium

We consider the case of a homogeneous porous layer on an impermeable sea bottom (see Fig. 1-a). The total water depth (i.e. between the impermeable bottom and the mean level at rest, corresponding to $z = 0$) is denoted h [m]. In the general case, h varies in space as a function of the horizontal coordinates (x, y). The thickness of the porous medium layer (above the rigid bottom) is denoted $h_p = \alpha h$ [m], and also varies with (x, y) in the general case. Therefore, the thickness of the pure water layer above the porous medium is $h_w = h - h_p = (1 - \alpha)\, h = \beta h$ [m]. The parameters α [-] and β [-], both varying between 0 and 1 and such that $\alpha + \beta = 1$, therefore represent the fractions of the water column height occupied by the porous medium and the pure water, respectively.

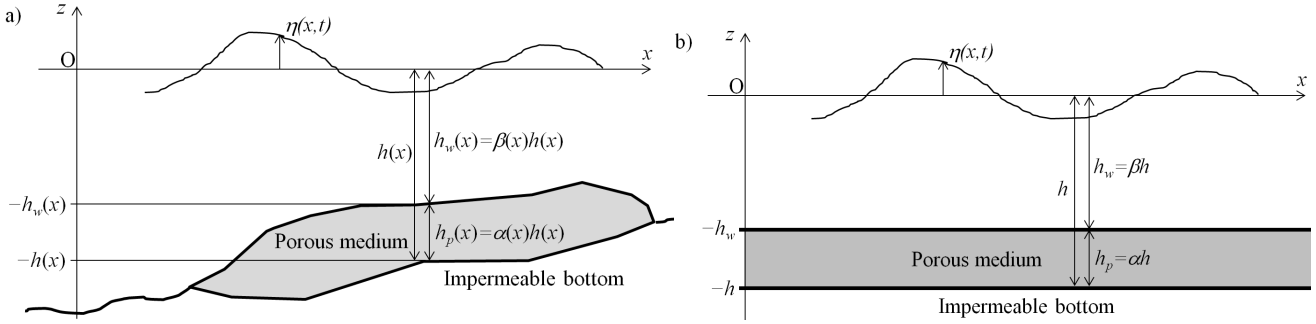

Fig. 1. Definition sketch of the problem studied here, with a lower layer of porous medium on an impermeable bed, and an upper layer of pure water. Panel a) general configuration with variable water depth and porous layer height; Panel b) particular case of infinite medium with uniform water depth and porous layer height.

Solitt and Cross (1972) developed a model of the flow inside the porous medium based on a potential approach. According to this model, the porous medium is characterized by the following set of parameters:

- porosity coefficients: the volume porosity $\hat{\tau}$ [-] is defined as the fraction of the total volume of porous medium occupied by water, and the surface porosity $\hat{\varepsilon} = 1 - (1 - \hat{\tau})^{2/3}$ [-] has to be considered when writing flow continuity equation at the interface between the porous medium and the water layer (see Eq. (3.f) below). Both porosity coefficients vary between 0 and 1.
- a coefficient of inertia $\hat{S} = 1 + C_a (1 - \hat{\tau}) / \hat{\tau}$ [-], where C_a [-] is a coefficient of added mass.
- a linearized friction coefficient $\hat{f}$ [-].

Here, these parameters are assumed to be constant inside the whole porous layer. Furthermore, we define $\hat{\phi} = \hat{\varepsilon} / (\hat{S} - i\hat{f})$ a (complex) parameter combining the characteristics of the porous medium.

The free surface elevation, measured with respect to the level at rest ($z = 0$), is denoted by $\eta(x, y, t)$ [m], and we denote $\Phi(x, y, t)$ [m^2/s] and $\Psi(x, y, t)$ [m^2/s] the potentials in the water layer and in the porous medium, respectively. In the following, we assume the problem is invariant along the y direction and that the waves propagate along the x direction to simplify the presentation, limiting ourselves to 2DV cases (x, z). The surface waves are assumed to have small amplitude so that a linear modeling approach can be used. We furthermore consider monochromatic waves with (known) wave period T [s] and angular frequency $\omega = 2\pi / T$ [rad/s].

The pressure in the upper water layer is given by the Bernoulli equation (here linearized):

$$\frac{p_w}{\rho}(x,z,t) = -\Phi_t - gz \qquad -h_w(x) \le z \le 0 \tag{1}$$

where ρ is the water density and g the acceleration due to gravity. In the porous layer, the pressure is given by a generalized Bernoulli relation (e.g. Losada et al., 2016):

$$\frac{p_p}{\rho}(x,z,t) = -\hat{S}\Psi_t - gz - \omega\hat{f}\,\Psi \qquad -h(x) \le z \le -h_w(x) \tag{2}$$

taking into account inertia effects through the coefficient $\hat{S}$ in the first term of the right hand side (RHS) and a linearized friction term using the friction coefficient $\hat{f}$ (last term of the RHS of Eq. (2)).

The problem is defined by the following set of equations:

$$\Phi_{xx} + \Phi_{zz} = 0 \qquad -h_w(x) \le z \le 0 \tag{3.a}$$

$$\Psi_{xx} + \Psi_{zz} = 0 \qquad -h(x) \le z \le -h_w(x) \tag{3.b}$$

$$\Phi_t = -g\eta \qquad z = 0 \tag{3.c}$$

$$\eta_t = \Phi_z \qquad z = 0 \tag{3.d}$$

$$\Psi_z + h_x \Psi_x = 0 \qquad z = -h(x) \tag{3.e}$$

$$\frac{\partial \Phi}{\partial \vec{n}} = \hat{\varepsilon} \frac{\partial \Psi}{\partial \vec{n}} \qquad z = -h_w(x) \tag{3.f}$$

$$\Phi_t = \hat{S}\Psi_t + \omega \hat{f}\,\Psi \qquad z = -h_w(x) \tag{3.g}$$

Eqs. (3.a) and (3.b) express mass conservation in the water layer and in the porous layer, respectively. Eq. (3.c) is the (linearized) dynamic free surface boundary condition (FSBC), while Eq. (3.d) is the (linearized) kinematic FSBC. Eq. (3.e) is the impermeability bottom boundary condition. Eq. (3.f) expresses the continuity of the flow discharge at the interface between the two layers, relating to the normal velocity at the interface and taking into account the porosity of the porous medium ($\vec{n}$ is the unit vector normal to the interface). Finally, Eq. (3.g) expresses the continuity of pressure at the interface. In principle, this system must be supplemented with lateral boundary conditions.

2.2 Analytical solution for the case of uniform water depth and porous layer height

Considering the particular case of progressive linear waves in an infinite domain in the x direction with constant water depth h and constant porous medium height h_p (as depicted in Fig. 1-b), the free surface elevation can be written in the following form:

$$\eta(x,t) = \mathrm{Re}\left\{ a \exp\left(i(\omega t - Kx)\right) \right\} = \exp\left(K_i x\right) \mathrm{Re}\left\{ a \exp\left(i(\omega t - K_r x)\right) \right\} \tag{4}$$

where $K = K_r + \mathrm{i}K_i$ is the wave-number, a complex quantity in the general case. *A priori*, there are several possible solutions for this wave-number, denoted as K_n (n = 0, 1, 2, ...). The real part of each K_n, $K_{nr} = \mathrm{Re}\{K_n\}$, gives the wavelength of the waves $L_n = 2\pi/K_{nr}$ [m], and the imaginary part $K_{ni} = \mathrm{Im}\{K_n\}$ corresponds to the rate of attenuation of the waves in space, given by the term $\exp\left(K_i x\right)$ in Eq. (4), with the condition that $K_{ni} \le 0$ due to the form chosen here for the solution (4).

In this situation, the problem can be solved analytically and a dispersion relation can be derived (e.g. Losada et al., 1996), expressed as:

$$\hat{\phi}\tanh(Kh_p)\left(1 - \frac{\omega^2}{gK}\tanh(Kh_w)\right) = \frac{\omega^2}{gK} - \tanh(Kh_w) \tag{5.a}$$

or equivalently, by denoting $X \equiv Kh$ [-] and $\Gamma \equiv \dfrac{\omega^2 h}{g}$ [-]:

$$F(X,\Gamma,\alpha,\hat{\varphi}) \equiv \Gamma - X\tanh(\beta X) - \hat{\varphi}\tanh(\alpha X)\left[X - \Gamma\tanh(\beta X)\right] = 0 \tag{5.b}$$

Determining all the roots of Eqs. (5.a) or (5.b) is a difficult numerical problem in the general case, as reported by several authors (Losada et al., 1996; Mendez and Losada, 2004; Chang and Liou, 2006). It would seem natural to use an iterative method to solve these equations. However, starting from the solutions of the classical wave dispersion relation without porous medium, these authors have shown that iterative methods of Newton-type or Müller-type do not systematically converge to the correct solutions. In the present work, we have followed the homotopy technique introduced by Chang and Liou (2006) to solve Eq. (5.b). For each wave-number K, the solution for the potential in each layer is then obtained as:

$$\Phi(x,z,t) = i\frac{g}{\omega}\eta(x,t)F(z) \qquad -h_w(x) \le z \le 0 \tag{6.a}$$

$$\Psi(x,z,t) = i\frac{g}{\omega}\eta(x,t)G(z) \qquad -h(x) \le z \le -h_w(x) \tag{6.b}$$

with $F(z)=\cosh(Kz)+\frac{\omega^2}{gK}\sinh(Kz)$ and $G(z)=\frac{\frac{\omega^2}{gK}\cosh(Kh_w)-\sinh(Kh_w)}{\hat{\varepsilon}\sinh(Kh_p)}\cosh(K(h+z))$ (6.c)

In order to apply this solution, the parameters of the porous medium (namely $\hat{\varepsilon}$, $\hat{S}$ and $\hat{f}$) appearing in the coefficient $\hat{\phi}$ need to be determined, which is the purpose of the next section.

3 Experimental characterization of cages of oyster shells as a porous medium

3.1 Experimental setup for hexapod tests

With the aim to determine the values of the physical parameters representative of the COS considered as a porous medium, an extensive experimental campaign was conducted in an hexapod facility at Centrale Marseille in standing waves conditions. This hexapod is a motion generator with 6 degrees of freedom (DOF). It allows, using a system of computer-controlled actuators, to impose simple or combined movements according to one or more of the 6 DOF to an object fixed on its tray. It allows to study objects with a maximum mass of one ton and to impose acceleration up to 1 times the gravity acceleration. Here, the hexapod imposes regular surge motions with small amplitude of a parallelepipedic tank containing one or several COS immersed in water (see Fig. 2).

Recently, similar tests have been carried out in this facility with a rectangular tank filled with a large number of vertical cylinders piercing the free surface or completely immersed (Molin et al., 2016), and a similar methodology is followed here. The tank is subjected to translational movements at frequencies close to the natural frequency of the first sloshing mode. The measurements consist of the elevation of free surface at the lateral walls of the tank and the hydrodynamic forces recorded by the 6 actuators of the hexapod, which make it possible to have access at any time to the full set of forces and torques. Using a similar theoretical approach as the one outlined in Section 2 (linear potential flow approach including a friction term in the porous layer to express the energy dissipation due to the viscous effects in the porous medium) but now considering standing waves in the tank, a modal approach is applied to represent the sloshing wave motion.

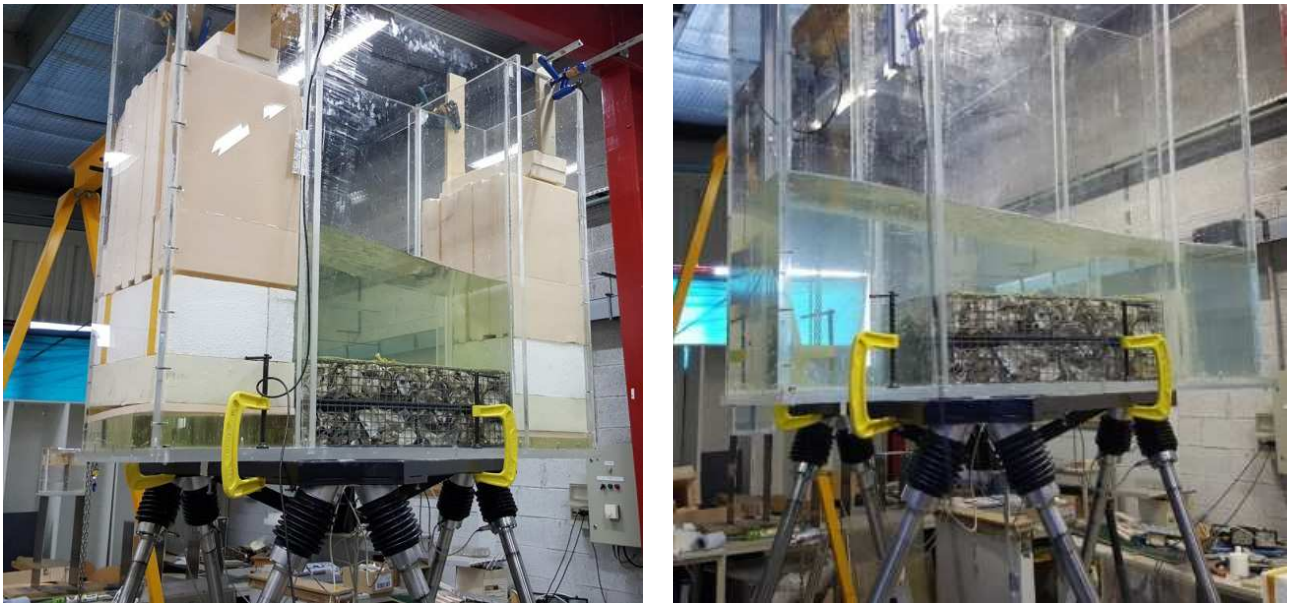

Fig. 2. Photographs of the test setup in the hexapod. Panel a) configuration A with COS occupying the full effective length of the tank (which is about half of the total length of the tank); Panel b) configuration B with COS occupying half the length of the tank (here COS centered in the middle of the tank)

In this work, the COS unit considered have the following dimensions: 0.80 m (length) x 0.50 m (width) x 0.12 m (height). Photographs of these COS units are given in Fig. 2. First, the volume porosity of the COS was determined by measuring the excess volume of water when a COS is immersed in a tank already filled with water. A value $\hat{\tau}$ = 80% was obtained with a variability of about ± 1.5%, after 5 tests on different COS units.

The testing tank, built for the present study, has a rectangular base of 1.60 x 0.51 m. Its height is large to prevent water from coming out of the tank during testing, especially for testing around the natural frequency. Two configurations were tested:

- Configuration A (or "small tank") corresponding to COS occupying the entire length of the tank (see Fig. 2-a). In this case, the tank is compartmentalized and the useful length is reduced to 0.82 m (i.e. slightly larger than the length of the COS). The two compartments on the sides (not used) are filled with polystyrene in order to limit the weight of the onboard water and the bias on the measurements of forces that would generate movements of the fluid in these compartments.
- Configuration B (or "large tank") corresponding to COS occupying half the length of the tank, located either in the middle of it or on one side. In both cases, the length filled with water is 1.60 m (see Fig. 2-b).

In the following, only results of configuration A are considered for determining the parameters of the porous medium.

3.2 Measurements and analysis of hexapod test results

For a range of water depths and forcing periods, the Response Amplitude Operator (RAO) of the amplitude of the waves on the lateral walls is measured, as well as the forces and torques exerted by the tested structure on the oscillating platform, from which a damping coefficient, denoted C_b, is determined (details of the method can be found in Molin et al. (2016). Using the values determined above for the porosity ($\hat{\tau}$ = 80% and $\hat{\varepsilon}$ = 66%), the values of the added-mass coefficient C_a and the friction coefficient $\hat{f}$ are determined so that experimental curves of the RAO and C_b match as closely as possible the curves given by the numerical model. Examples of such comparison between experimental results and numerical predictions are given in Fig. 3 (RAO curves) and Fig. 4 (Cb curves) for a particular case of one single COS (h_p = 0.12 m) in a water depth h = 2 h_p = 0.24 m. Two experimental curves are plotted, corresponding to 1 mm and 2 mm of amplitude of surge motion imposed by the hexapod. Due to lower influence of nonlinearity, tests with 1 mm of motion amplitude are usually preferred to determine the parameters.

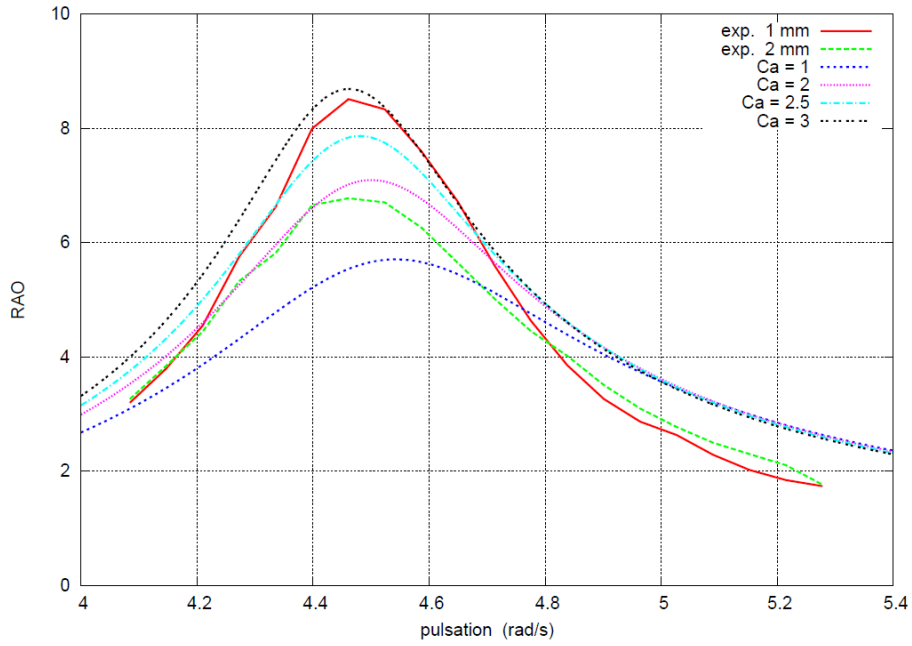

Fig. 3. RAO of the free surface elevation in the tank (hexapod experiments) for the case h_p = 0.12 m (one single COS) in a water depth h = 2 h_p = 0.24 m. Regarding the curves from the numerical model, the value of the friction coefficient is fixed ($\hat{f}$ = 1) and various values of C_a are tested.

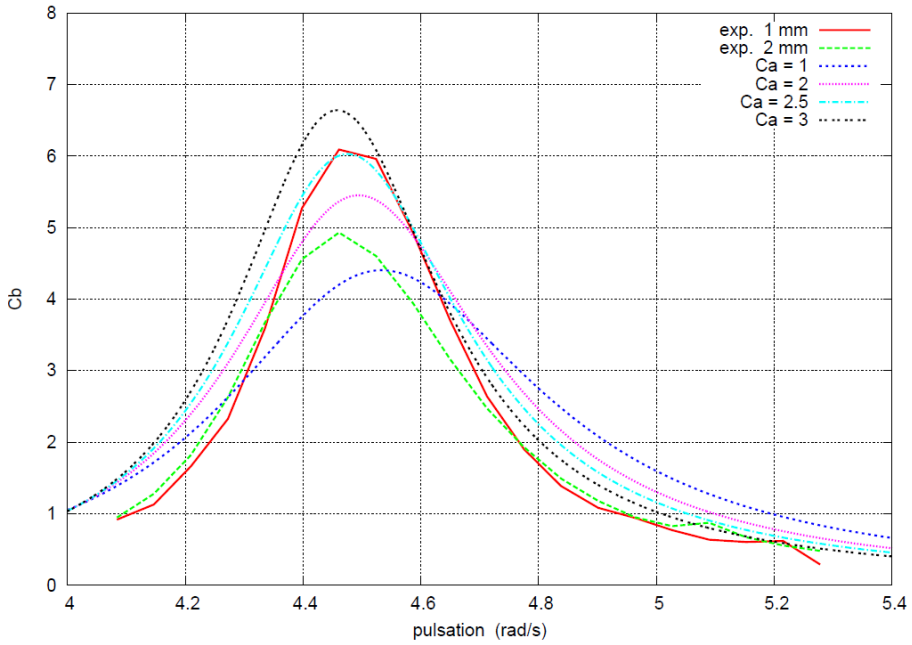

Fig. 4. Damping coefficient C_b of the free surface elevation in the tank (hexapod experiments) for the case $h_p = 0.12$ m (one single COS) in a water depth $h = 2\ h_p = 0.24$ m. Regarding the curves from the numerical model, the value of the friction coefficient is fixed ($\hat{f} = 1$) and various values of C_a are tested.

In the results plotted in Figs 3 and 4, the value of the friction coefficient is fixed to $\hat{f} = 1$, which appeared to be the optimal value, at least for this amplitude of motion of the tank (not shown here). Various values of C_a are then tested, and it appears that $C_a = 2.5$ produces a best fit of the two curves.

The set of values ($\hat{f} = 1$, $C_a = 2.5$) was tested on all other configurations studied in the hexapod (with configuration A). In general, the agreement reached appeared reasonable given that oyster shells have specific characteristics (compared to classical rip rap): it is a strongly anisotropic medium (*a priori*, there are more shells in the horizontal direction than in the vertical direction, the effects of added mass in both directions are not strictly identical), and the shells have many sharp angles.

It is generally observed that the coefficient of friction $\hat{f}$ must be taken larger (around 1.4) for tests performed with an amplitude of motion 2 mm, compared to tests with an amplitude of 1 mm, for which $\hat{f} = 1$ generally gives the good order of magnitude of the experimental curves. The fact that the coefficient $\hat{f}$ must be adjusted according to the amplitude of the imposed motion is a clear sign that damping forces have a non-negligible quadratic component. This one is not taken into account in the current version of the theoretical model (which only considers a linearized friction force). Going further in the analysis and taking into account of these effects would require testing other formulations of frictional forces, which is left for future studies.

4 Numerical models for waves interacting with a series of COS in variable bottom conditions

4.1 Deterministic modeling of wave transformation with porous medium and variable depth

In order to model wave transformation in the presence of a porous layer close to the bottom in variable depth conditions (as depicted schematically in Fig 1-b), we follow Rojanakamthorn et al. (1990) and Losada et al. (1996). These authors derived an approximate model for monochromatic waves within the framework of linear potential formalism, assuming mild slopes of the bottom elevation and of the porous layer height. This model is similar in spirit to the mild slope equation derived by Berkhoff (1972). The system of initial equations is the system of Eqs.(3.a – 3.g) presented in Section 2.

As the total water depth h and height of porous layer h_p vary smoothly and slowly with the position (x, y), it is assumed (i) that the vertical dependence of the potential remains the same as that obtained in the case of a uniform medium treated in sub-section 2.2 and given by Eq. (6.c), and (ii) that the local values of the (complex) wave-number $K(x, y)$ and (complex) phase celerity $C(x, y) \equiv \omega/K$ are given by the dispersion relation in uniform medium (Eqs. (5.a) or (5.b)), but using local values of $h_w(x, y)$, $h_p(x, y)$ and $h(x, y)$.

An additional hypothesis of the model is to retain in the solution only the first mode (mode 0, giving K_0 for the wave-number), similar to the propagative mode for the case without porous medium, and to ignore all the higher modes. This simplification is supported by the locations of wave-numbers K_n in the complex plane, which show that wave-numbers K_n for $n \geq 1$ have larger imaginary parts, and thus behave essentially as local (evanescent) modes (not shown here).

Following Eqs. (6.a) and (6.b), the potentials in the two layers are written as:

$$\Phi(x,y,z,t) = \bar{\phi}(x,y,t)F(z) = \left(i\frac{g}{\omega}\hat{\eta}(x,y)e^{i\omega t} \right) F(z) \qquad -h_w(x,y) \leq z \leq 0 \tag{7.a}$$

$$\Psi(x,y,z,t) = \bar{\phi}(x,y,t)G(z) = \left(i\frac{g}{\omega}\hat{\eta}(x,y)e^{i\omega t} \right) G(z) \qquad -h(x,y) \leq z \leq -h_w(x,y) \tag{7.b}$$

and it can be shown under the above assumptions that $\hat{\eta}(x,y)$ satisfies the following elliptic-type mild slope equation (EMS), formulated in the three equivalent forms as:

$$\nabla \cdot \left(n_0 C_0^2 \nabla \hat{\eta} \right) + n_0 \omega^2 \hat{\eta} = 0 \tag{8.a}$$

$$\nabla \cdot \left(\beta_0 \nabla \hat{\eta} \right) + K_0^2 \, \beta_0 \hat{\eta} = 0 \tag{8.b}$$

$$\Delta \hat{\eta} + \frac{\nabla \beta_0}{\beta_0} . \nabla \hat{\eta} + K_0^2 \, \hat{\eta} = 0 \tag{8.c}$$

where $n_0 \equiv \frac{1}{2}\left(1 + \frac{2K_0 h}{\sinh(2K_0 h)} \right)$ and $\beta_0 \equiv n_0 C_0^2$ are quantities varying in (x,y), but constant in time. Note that these terms correspond respectively to C_g/C and CC_g for the classical mild slope equation without porous medium, but they are here complex quantities. For the 1DH case, we will subsequently solve this EMS model under the form of Eq. (8.c):

$$\hat{\eta}_{xx} + \frac{(\beta_0)_x}{\beta_0} \hat{\eta}_x + K_0^2 \, \hat{\eta} = 0 \tag{9}$$

4.2 Phase-averaged modeling of wave transformation with porous medium and variable depth

Eq. (8) is a deterministic (phase-resolving) model: its numerical simulation requires choosing a grid size of about 1/10 of the local wavelength. It is therefore desirable to examine whether a phase-averaged model (not subjected to the same discretization constraint) could be applied as well. To that end, we assume that the waves are essentially progressive and write the complex amplitude as:

$$\hat{\eta}(x,y) = a(x,y)\exp\left(-i\theta(x,y)\right) \tag{10}$$

where $a(x,y)$ is the wave amplitude [m] and $\theta(x,y)$ its phase [rad]. We also write the complex term β_0 as $\beta_0 \equiv B\exp(i\psi)$, where $B = |\beta_0|$ et $\psi = \mathrm{Arg}(\beta_0)$ are the modulus and phase of β_0 respectively, and define $\vec{\kappa} \equiv \nabla\theta$ the wave-number vector. We further denote $K_0 \equiv K_r + iK_i$. After inserting Eq. (10) into Eq. (8) and separating the real and imaginary parts, we obtain after some calculations:

$$\kappa^2 = K_r^2 - K_i^2 + \frac{\Delta a}{a} + \frac{\nabla B}{B} . \frac{\nabla a}{a} + \vec{\kappa} . \nabla\psi \tag{11.a}$$

$$\nabla . \left(B\vec{\kappa}E \right) = B\left(2K_r K_i \, E + \frac{1}{2}\nabla\psi . \nabla E \right) \tag{11.b}$$

Eq. (11.a), known as the eikonal equation, gives the modulus of the wave-number vector, being recalled that this vector also satisfies the irrotationality condition $\nabla \times \vec{\kappa} = \vec{0}$. Eq. (11.b) is an equation on the wave energy flux $B\vec{\kappa}E$, where $E = \frac{1}{2}\rho g a^2$ is the average wave energy per unit surface in the horizontal plane. Note Eqs. (11.a) and (11.b), called "**system 1**", still form a phase-resolving model.

While searching for simplified versions of system 1, an analysis of order of magnitudes of the various terms in the RHS of Eqs. (11.a) and (11.b) was carried out, and it appeared that the first term in each of these equations represents usually the dominant contribution, so that after neglecting the other terms the eikonal Eq. (11.a) reduces to $\kappa \approx K_r$ and Eq. (11.b) can then be approximated as a model, called "**system 2**", written below for the 1DH case:

$$\left(BK_r a^2\right)_x = 2K_r K_i\, Ba^2 \tag{12}$$

This system 2 is now a phase-averaged model, whose numerical simulation is easier than both the EMS and system 1, and it can be discretized using coarser grids. However, this system does not account for physical processes related to the changes of wave phase, in particular diffraction and reflection effects are not present in this model. One can also note that the dissipation of energy in the RHS of Eq. (12) is mainly controlled by the imaginary part K_i of the wave-number K_0.

5 Validation of the numerical models through wave flume tests with series of COS

5.1 Experimental set-up of wave flume experiments with series of COS

The models derived in Section 4 were then applied to a set of laboratory tests carried out independently in a wave flume at EDF R&D, Chatou (France). The wave flume is 72 m long. In the absence of COS, the bottom of the flume was flat, and 3 values of the water depth h were considered: 0.50 m, 0.67 m and 0.83 m. Tests were performed in irregular unidirectional wave conditions, characterized by a significant height H_s [m] and a peak period T_p [s].

In these tests, various arrangements of the same type of COS as used during the hexapod tests were considered. Three different heights of COS were tested, stacking 1, 2 or 3 units of 0.12 m height each. In the longitudinal direction (along the flume centerline) the extent of each COS zone is 0.50 m. The COS are not contiguous, but spaced with a separation distance of 0.30 m.

In total, 16 tests were performed by EDF R&D:

- 9 tests with 25 COS zones: 0.50 m long and 0.24 m high, spaced 0.30 m apart,
- 4 tests with 16 COS zones: 0.50 m long and 0.36 m high, spaced 0.30 m apart,
- 3 tests with 25 COS zones: 0.50 m long and 0.12 m high, spaced 0.30 m apart.

A series of 20 wave measurement probes were deployed along the wave flume. Sensors #1 to #5, located between the wave generator and the first COS area, were used to separate incident and reflected wave trains. Sensors #6 to #20 were set over the domain covered by the COS, and after these COS, with the convention that the origin of the x-coordinates is set at the beginning of the first COS zone, also corresponding to the position of sensor # 6. The positions of these probes are given in Table 1. After the experiments, it was observed that data from probes #9 and #17 were not always reliable; therefore, these two probes were discarded from the analysis and comparisons.

Tab. 1. Position of the wave measurement probes used during the wave flume experiments.

Probe number	Position w.r.t. wave flume origin [m]	Distance from previous probe [m]	Abscissa used for modeling [m]	Comments
6	38.30		0.00	Position of the start of the first COS
7	36.80	1.50	1.50	
8	35.25	1.55	3.05	
9	33.65	1.60	4.65	*Probe out of order (not used)*
10	32.15	1.50	6.15	
11	30.60	1.55	7.70	
12	29.05	1.55	9.25	
13	27.50	1.55	10.80	
14	25.90	1.60	12.40	
15	24.45	1.45	13.85	
16	22.90	1.55	15.40	
17	21.30	1.60	17.00	*Probe out of order (not used)*
18	19.80	1.50	18.50	
19	18.30	1.50	20.00	Position of the end of the last COS
20	16.70	1.60	21.60	

5.2 *Numerical modeling settings and discretization*

As mentioned in the previous sub-section, the tests were performed with irregular waves, but they are simulated numerically with both the EMS model (Eq. (9)) and system 2 (Eq. (12)) using monochromatic waves, taking for the wave height $H = H_s$ and for the period $T = T_p$. The values actually used for H_s and T_p are recalled in the legends of the figures of results below.

The two models use the same 1DH spatial mesh, from x = -2.5 m to 22.5 m, with a uniform resolution Δx = 0.01 m (i.e. 2501 nodes in total). A COS unit (length of 0.50 m) thus corresponds to 50 grid cells. Note that, in order to limit the numerical effects linked to the rectangular shape of the COS, their geometry was slightly smoothed in the numerical models by imposing a smooth transition of the COS height between 0 and h_p over 5 nodes at the beginning and end of each COS.

The parameters of the porous medium of the COS are deduced from the tests carried out in the hexapod (see Section 3):

- volume porosity $\hat{\tau} = 0.80$, giving a surface porosity $\hat{\varepsilon} = 0.66$,
- added mass coefficient Ca = 2.50, giving a coefficient of inertia $\hat{S}_f = 1.625$.
- linearized friction coefficient $f = 0.8$. Compared to the value $f = 1$ obtained in Section 3, a slight reduction was observed to improve the comparison with the wave flume experiments.

5.3 *Comparison of results for 25 COS zones with height h_p = 0.24 m (2 COS units stacked)*

Comparisons for the case of 25 COS zones with height $h_p = 0.24$ m (2 unit COS stacked) are presented in Figs. 5 and 6 for two hydrodynamic conditions. In both cases, the comparison with the measurements confirms the relevance of the proposed models. The measured decay rate of wave height and energy as waves propagate over a series of COS is well captured by the two models.

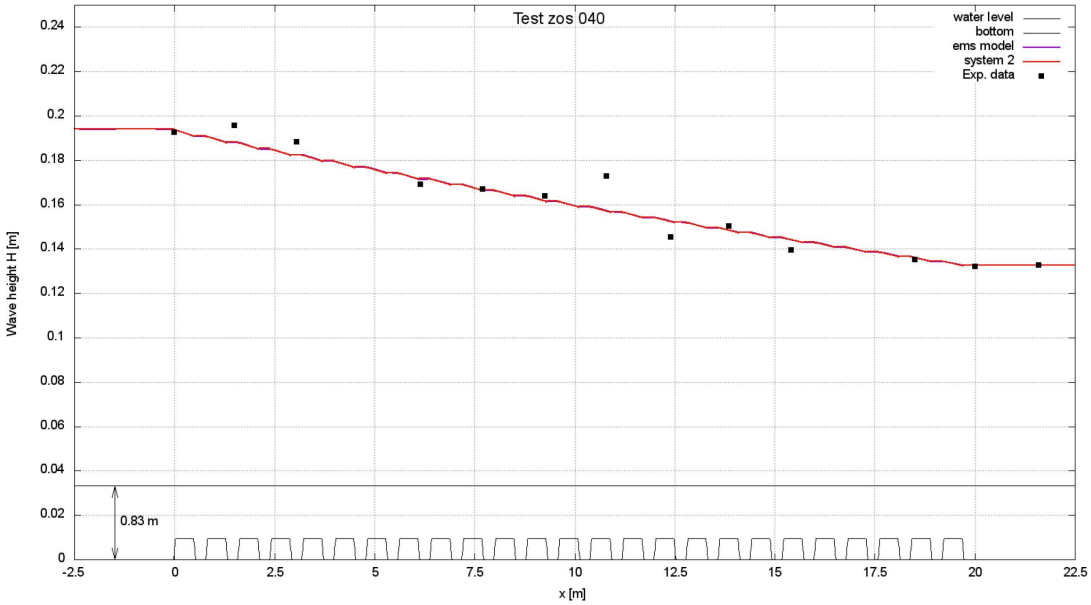

Fig. 5. Simulation of wave height evolution for a test with 25 successive COS each of height h_p = 0.24 m in a water depth h = 0.83 m with irregular incident waves: H_s = 0.20 m and T_p = 1.67 s. The purple curve (EMS) is the result from the elliptic mild slope model and the red curve is the result from the simplified phase-averaged model (system 2). Black squares represent measured wave heights at various positions along the wave flume.

For the case presented in Fig. 5, corresponding to both shorter waves (T_p = 1.67 s) and deeper water conditions (h = 0.83 m), the attenuation due to the COS zones is lower, and differences between the two models are weak. For the case presented in Fig. 6 with longer waves (T_p = 2.48 s) and lower water depth (h = 0.50 m), the wave dissipation is stronger, resulting in lower transmission coefficients. For this case, where reflection effects are more significant, differences between the two models are more marked. The curve of system 2 results exhibits a crenelated (rectangular) shape following the succession of COS zones. The EMS model, superior in representing reflection and diffraction effects associated with each individual COS, produces a smoother wave height evolution. Note the transmitted wave heights are slightly different between the two models in this second case.

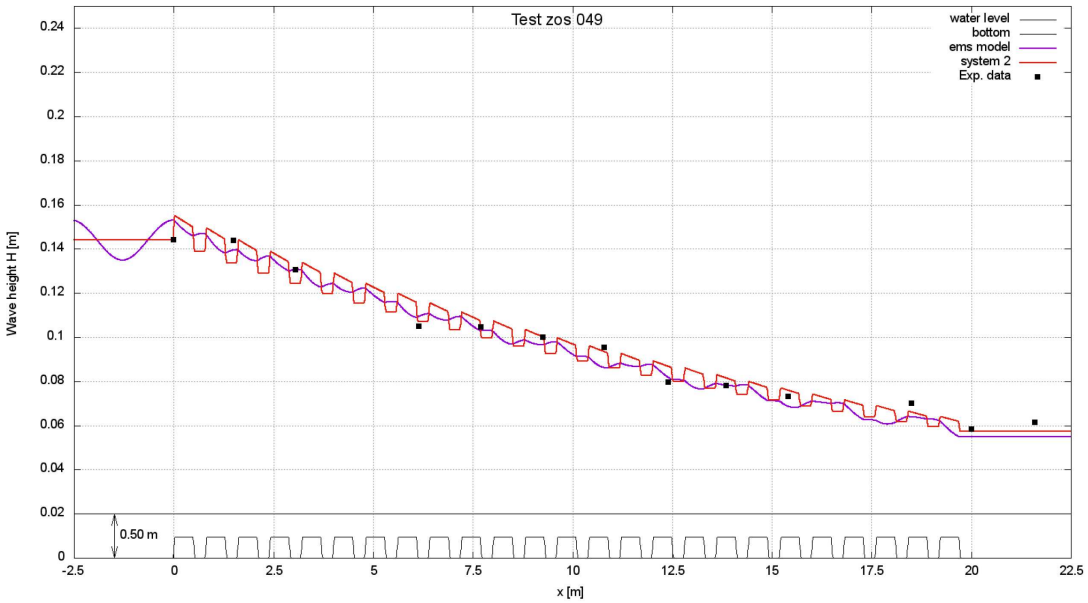

Fig. 6. Simulation of wave height evolution for a test with 25 successive COS zones each of height h_p = 0.24 m in a water depth h = 0.50 m with irregular incident waves: H_s = 0.15 m and T_p = 2.48 s. See legend of Fig. 5.

6 Discussion and conclusions

The combination of experiments and numerical simulations carried out during this study has allowed a better understanding of the ability of parallelepipedic metallic cages filled with used oyster shells (COS) to dissipate wave energy in shallow-water areas. It appears that these COS can be reasonably well represented by a layer of porous medium above the rigid bottom. The characteristics of this porous medium could be determined from a series of tests in an hexapod facility (sloshing wave motion in a tank containing one or several stacked COS).

In order to simulate the propagation of waves over a series of COS zones in variable depth conditions, a mild-slope type (phase-resolving) model originally introduced by Rojanakamthorn et al. (1990) and then used by Losada et al. (1996) was adopted. This model was then subsequently simplified into a phase-averaged equation, called “system 2”, in which the dissipative effect of the COS appears through the imaginary part of the wave-number. The results from these two models were compared with an independent series of experiments performed in a wave flume. An overall good agreement is obtained for both these models regarding wave height attenuation and transmission for a range of relative water depth conditions and various relative heights of the COS structures. Although the “system 2” model needs further validation in other conditions, it appears as a promising simplified model for engineering calculations of the effects of such COS devices.

References

Berkhoff, J.C.W., 1972. Computations of combined refraction-diffraction. Proceedings of the 13th International Conference on Coastal Engineering, ASCE, Vancouver (Canada), pp. 471-490.

Chang, H.-K., Liou, J.-C., 2006. Solving wave dispersion equation for dissipative media using Homotopy perturbation technique. Journal of Waterway, Port, Coastal, and Ocean Engineering, 132(1), 28–35.

Losada, I.J., Silva, R., Losada, M.A., 1996. 3-D non-breaking regular wave interaction with submerged breakwaters. Coastal Engineering, 28(1-4), 229–248.

Losada, I.J., Lara, J.L., del Jesus, M., 2016. Modeling the interaction of water waves with porous coastal structures. Journal of Waterway, Port, Coastal, and Ocean Engineering, 142(6), 03116003.

Mendez, F.J., Losada, I. J., 2004. A perturbation method to solve dispersion equations for water waves over dissipative media. Coastal Engineering, 51(1), 81–89.

Molin, B., Remy, F., Arnaud, G., Rey V., Touboul, J., Sous, D., 2016. On the dispersion equation for linear waves traveling through or over dense arrays of vertical cylinders. Applied Ocean Research, 61, 148–155.

Rojanakamthorn, S., Isobe, M.,Watanabe, A., 1990. Modeling of wave transformation on submerged breakwater. Proceedings of the 22th International Conference on Coastal Engineering, Delft (The Netherlands), pp. 1060–1073.

Sollitt, C.K., Cross, R.H. (1972) Wave transmission through permeable breakwaters. Proceedings of the 13th International Conference on Coastal Engineering, ASCE, Vancouver (Canada), pp. 1827–1846.